

CARNA: Characterizing Advanced heart failure Risk and hemodyNAMic phenotypes using learned multi-valued decision diagrams

Josephine Lamp, Yuxin Wu, Steven Lamp, Prince Afriyie, Kenneth Bilchick, Lu Feng, Sula Mazimba

arXiv:2306.06801v1 [cs.LG] 11 Jun 2023

Abstract—Early identification of high risk heart failure (HF) patients is key to timely allocation of life-saving therapies. Hemodynamic assessments can facilitate risk stratification and enhance understanding of HF trajectories. However, risk assessment for HF is a complex, multi-faceted decision-making process that can be challenging. Previous risk models for HF do not integrate invasive hemodynamics or support missing data, and use statistical methods prone to bias or machine learning methods that are not interpretable. To address these limitations, this paper presents CARNA (Characterizing Advanced heart failure Risk and hemodyNAMic phenotypes), a hemodynamic risk stratification and phenotyping framework for advanced HF that takes advantage of the explainability and expressivity of machine learned Multi-Valued Decision Diagrams (MVDDs). This interpretable framework learns risk scores that predict the probability of patient outcomes, and outputs descriptive patient phenotypes (sets of features and thresholds) that characterize each predicted risk score. Specifically, we develop an innovative methodology to first learn a risk stratification using hierarchical clustering, and develop a training regime to learn MVDDs that predict risk scores and output patient phenotypes. CARNA incorporates invasive hemodynamics and can make predictions on missing data. The CARNA models were trained and validated using a total of five advanced HF patient cohorts collected from previous trials, and compared with six established HF risk scores and three traditional ML risk models. CARNA provides robust risk stratification, outperforming all previous benchmarks. Although focused on advanced HF, the CARNA framework is general purpose and can be used to learn risk stratifications for other diseases and medical applications. Moreover, to facilitate practical use, we provide an extensible, open source tool implementation.

Index Terms—Explainable machine learning, heart failure, hemodynamics, multi-valued decision diagrams, phenotyping, risk stratification

This material is based upon work supported by the National Science Foundation Graduate Research Fellowship under Grant No. (1842490). This work was based on one of the winning solutions to the NHLBI Big Data Analysis Challenge: Creating New Paradigms for Heart Failure Research.

Josephine Lamp, Steven Lamp and Lu Feng are with the Department of Computer Science, University of Virginia, Charlottesville, VA, USA (e-mail: {jl4rj; vx3kr; lu.feng}@virginia.edu)

Yuxin Wu is with the Department of Computer Science, University of California, Los Angeles, CA, USA (e-mail: yuxinwu98611@g.ucla.edu)

Prince Afriyie is with the Department of Statistics, University of Virginia, Charlottesville, VA, USA (e-mail: pa5jg@virginia.edu)

Kenneth Bilchick and Sula Mazimba are with the Department of Cardiovascular Medicine, University of Virginia, Charlottesville, VA, USA (e-mail: {KCB7F; SM8SD}@uvahealth.org)

I. INTRODUCTION

HEART failure (HF) is a complex disease condition with high morbidity and mortality [1]. On a fundamental level, HF is defined by the inability of the heart to deliver adequate blood flow to the body without an elevation in cardiac filling pressures [2]. Identifying high risk advanced HF patients early on in the care continuum is critical for timely allocation of advanced, life-saving therapies such as mechanical support, device implantation or transplant allocation. Due to high variability in patient conditions and complexity of the disease, determining patient risk involves a challenging, multi-faceted decision making process that places a high burden on clinicians [3]. Hemodynamic assessments can facilitate risk stratification and enhance understanding of HF trajectories [4]. Hemodynamics provide measures of cardiovascular function, and quantify distributions of pressures and flows within the heart and circulatory system [5]. However, obtaining a comprehensive picture of the patient state from these, particularly in the context of treatment-guiding outcomes, is difficult [6].

Many established HF risk scores such as the Seattle Heart Failure Risk model [7] use statistical or naive models which are difficult to optimize and may be prone to bias [8]–[10]. Machine learning (ML) models present a promising opportunity to outperform traditional risk assessment methods, especially when dealing with large, high-dimensional data [11]. However, despite the promise of machine learning for HF risk stratification, ML-based risk scores remain unpopular due to modest model performance and issues with model interpretability [12]. Moreover, no previous models (statistical or ML-based) incorporate invasive hemodynamics, or contain mechanisms to handle missing data.

To address these limitations, this paper develops and validates an advanced HF hemodynamic risk stratification framework entitled CARNA (Characterizing Advanced heart failure Risk and hemodyNAMic phenotypes)¹. We harness the explainability and expressivity of machine learned Multi-Valued Decision Diagrams (MVDDs) to learn a risk score that predicts the probability of patient outcomes, including mortality and rehospitalization, and provide descriptive patient phenotypes. MVDDs are discrete structures representing logical functions in directed, acyclic graphs where nodes represent features, edges represent logical operators (“and”, “or”) with parameter

¹So named for the roman healing goddess who presides over the heart.

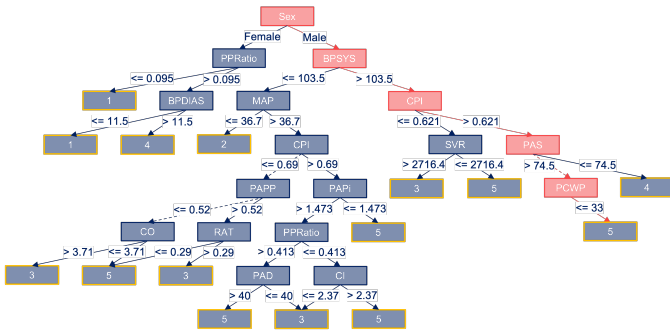


Fig. 1: Example MVDD for the Invasive Hemodynamic Feature Set and DeLvTx Outcome. Dotted lines represent “or” boolean operators, and solid lines represent “and” boolean operators. The leaf nodes highlighted in yellow indicate the risk score. The highlighted red path indicates the example phenotype of $\text{Sex} = \text{Male} \wedge \text{BPSYS} > 103.5 \wedge \text{CPI} > 0.621 \wedge (\text{PAS} > 74.5 \vee \text{PCWP} \leq 33) = \text{Score } 5$.

threshold values, and leaf nodes represent the final score classification [13]. An example MVDD is shown in Figure 1. Due to their use of logical operators, MVDDs can handle missing data, as multiple substitutable features may contribute to the same score prediction. Moreover, the “path” through the MVDD may be returned to provide a descriptive patient phenotype that characterizes the score. MVDDs have typically been applied in optimization and model checking contexts [14], and they do not inherently learn a risk stratification. Therefore, we develop an innovative methodology within our framework to first learn a risk stratification using a hierarchical clustering algorithm, and then develop a training regime to train the MVDDs on the learned risk scores and output explainable phenotypes. Although focused on advanced HF, CARNA is a general purpose risk stratification and phenotyping framework that can be used for other diseases and medical applications.

In summary, we present the following contributions:

- 1) We develop CARNA, an interpretable ML framework using Multi-Valued Decision Diagrams that works with missing data and includes invasive hemodynamics for risk stratifying advanced heart failure patients. In addition to producing a risk score, CARNA provides detailed patient phenotypes, i.e., sets of features and their thresholds that characterize a risk score.
- 2) We provide robust validation of the CARNA models using four independent HF cohorts, and compare them with six established HF risk scores and three traditional ML models. The CARNA models achieve high performance and outperform all benchmarks across metrics including Accuracy, Sensitivity, Specificity and AUC.
- 3) In order to facilitate practical use and promote open science, we provide an extensible, open-source tool implementation such that others can quickly and easily explore, extend, or prototype on top of the tool. In addition, our tool includes a deployed web server, which provisions live risk score prediction for ease of clinical use. All code is publicly available: <https://github.com/jozieLamp/CARNA>.

TABLE I: Comparison of HF Risk Score Approaches

| Score | Method Used | # Features | Hemo? | Allows Missing Data |
|---------------|----------------------|------------|-------|---------------------|
| CARNA Hemo | MVDD | 28 | Yes | Yes |
| CARNA All Fts | MVDD | 66 | Yes | Yes |
| EFFECT [20] | Logistic Regression | 11 | No | No |
| GWVG [21] | Logistic Regression | 7 | No | No |
| MAGGIC [22] | Poisson Regression | 13 | No | No |
| ESCAPE [23] | CPH | 8 | No | No |
| SHFM [7] | CPH | 30 | No | No |
| ADHERE [24] | Decision Tree (CART) | 3 | No | No |
| MARKER [25] | Decision Tree (BDT) | 8 | No | No |
| TOPCAT [26] | Various ML | 86 | No | No |

Hemo = Invasive Hemodynamics; All Fts = All Features; CPH = Cox Proportional Hazards; CART = Classification and Regression Tree; BDT = Boosted Decision Tree

[//github.com/jozieLamp/CARNA](https://github.com/jozieLamp/CARNA).

II. RELATED WORK

A. Explainable AI in Healthcare

Explainable AI (XAI) encompasses a wide range of techniques to provide interpretable explanations about a model’s choices, such as through the use of feature maps, textual annotations, local, feature or example explanations, and model simplification methods [15]. XAI methods have been used in a range of healthcare applications [16], including for predicting heart failure incidence [17]. Adding explainability to a model often comes with a trade-off: the XAI methods may be complicated to implement, inefficient (i.e., it takes much longer to train an explainable model), or have stability and reliability issues [18]. In addition, although these methods are good for understanding more about the model (e.g., visualizing at a high level how combinations of features contributed to a prediction), they are not always conducive to quick decision making in high stress environments. For example, interpreting feature maps or understanding textual explanations is nontrivial; one may need time to decipher the explanation and determine its use (e.g., figure out how a risk score was computed.) On the other hand, MVDDs are efficient, reliable and stable [19]. Moreover, they provide simple phenotypes that quickly summarize the exact set of features and thresholds that were used to make a score prediction. As such, they are easy to understand and provide an uncomplicated, quick decision support for clinicians during patient triage.

B. HF Risk Scores

There are a variety of HF risk scores that provide risk stratifications in HF populations using statistical and machine learning models; a comparison is available in Table I. The EFFECT [20], GWVG [21] and MAGGIC [22] risk scores predict risk of mortality in HF patients using various regression methods. The ESCAPE Risk Model and Discharge Score [23] and SHFM [7] stratify mortality risk using Cox Proportional Hazards models (CPH). The ESCAPE score was derived using the same dataset that we use for our training cohort. Finally, in the TOPCAT [26], ADHERE [24], and MARKER [25] risk models, machine learning algorithms, including decision trees, boosted decision trees, support vector machines and random forests are used to predict risk of mortality.

Some of these risk models use small, selective feature sets, or only stratify risk into a small number of groups (e.g., only

TABLE II: Characteristics of HF Cohorts

| | ESCAPE [27] | BEST [28] | GUIDE-IT [29] | UVA Shock | UVA Serial |
|-------------------------------|-------------|------------|---------------|------------|------------|
| # Patients | 433 | 2707 | 388 | 364 | 183 |
| # Patients with Invasive Hemo | 209 | 0 | 0 | 130 | 181 |
| Baseline Data | Yes | Yes | Yes | Yes | Yes |
| Discharge Data | Yes | No | Yes | Yes | Yes |
| Total Records | 866 | 2707 | 776 | 728 | 366 |
| Total Data Missing (%) | 7.8 | 2.0 | 15.1 | 10.4 | 7.3 |
| Hemodynamics Missing (%) | 12.0 | N/A | N/A | 5.9 | 9.2 |
| Age (years) | 56.1±13.9 | 60.2±12.3 | 62.2±13.9 | 59.4±18.5 | 60.6±15.1 |
| Sex (% female) | 25.9 | 21.9 | 66.2 | 35.2 | 43.2 |
| Race (% white) | 59.6 | 70.0 | 49.2 | N/A | N/A |
| BMI (kg/m ²) | 28.4±6.7 | N/A | 31.2±8.6 | 29.8±8.8 | 30.5±8.0 |
| LVEF (%) | 19.3±6.6 | 23.0±7.3 | 24.0±8.2 | 31.7±17.4 | 31.3±18.0 |
| SBP (mm Hg) | 103.7±15.8 | 118.5±19.4 | 115.4±20.0 | 111.1±21.9 | 109.1±21.4 |
| DBP (mm Hg) | 64.1±11.5 | 71.9±11.7 | 70.2±13.5 | 62.2±15.5 | 59.9±17.2 |
| Blood Urea Nitrogen (mg/dL) | 36.3±22.5 | 24.6±15.3 | 31.3±22.6 | 34.9±24.2 | 39.1±25.7 |
| Creatinine (mg/dL) | 1.5±0.6 | 1.2±0.4 | 1.6±0.7 | 1.7±1.3 | 1.7±1.0 |
| Potassium (mmol/L) | 4.3±0.6 | 4.3±0.5 | 4.4±0.6 | N/A | N/A |
| Sodium (mmol/L) | 136.0±4.4 | 138.9±3.4 | 138.3±3.8 | 136.9±5.1 | 135.7±5.2 |
| DeLvTx (%) | 27.0 | 31.7 | 23.7 | 56.6 | 41.5 |
| Rehospitalization (%) | 57.0 | 62.9 | 51.8 | 47.5 | 78.7 |

N/A indicates data not available; LVEF = ejection fraction; SBP = systolic blood pressure; DBP = diastolic blood pressure; DeLvTx = composite endpoint of death, LVAD implantation or transplantation.

two groups of high and low risk as in MARKER), and none of them incorporate invasive hemodynamics. Moreover, these methods suffer from limitations associated with statistical and naive machine learning models, such as being prone to bias, and lacking mechanisms to handle missing data [8], [9]. In fact, in external validation of these scores, a common issue cited is that some variables are not readily available in routine clinical practice or are missing from collected data cohorts so the score cannot be computed [10].

CARNA uses a larger, more diverse feature set than most scores, is able to provide more fine-grained risk stratification, i.e., can have more risk groups, and incorporates invasive hemodynamics. In addition, our model is explainable and can handle missing data. Ultimately, it is our intention that our risk score would be complementary to previous risk methodologies, in which our score is used to provision risk stratification for advanced HF patients requiring invasive hemodynamic monitoring, and others may be used to gain an understanding of risk for more general HF patients.

III. PRELIMINARIES

A. Multi-Valued Decision Diagrams

MVDDs are discrete structures representing logical functions in directed, acyclic graphs where nodes represent features, edges represent logical operators (“and”, “or”) with parameter threshold values, and leaf nodes represent the final score classification [13]. As such, the “path” through the graph may be returned to provide a descriptive patient phenotype. An example MVDD is shown in Figure 1: the highlighted red path characterizes the high-risk score of 5 by the following phenotype: $Sex = Male \wedge BPSYS > 103.5 \wedge CPI > 0.621 \wedge (PAS > 74.5 \vee PCWP \leq 33) = Score 5$.

MVDDs are well suited to classification tasks and the representation of HF phenotypes over other black-box models because they allow increased flexibility in characterizing

feature relationships and are highly interpretable [19]. This is advantageous over other models that do not provide any details about how a score was computed. Moreover, unlike other explainable models such as decision trees or random forests, MVDDs are resilient to missing data due to their use of logical operators; multiple substitutable features may contribute to the same prediction score. For example, in the above phenotype, PAS or PCWP may be used for calculation, and as such, when a feature is missing from the provided data, alternative features may be used to still allow for score prediction. This is advantageous in clinical scenarios where complete patient measurements may not be available and clinicians must make quick decisions on partial observations.

Despite these advantages, MVDDs have typically been used for optimization and model checking contexts [14], with limited use in medical classification and no applications to risk stratification. As such, we develop a training regime for MVDDs within our framework to learn risk scores and output HF phenotypes that characterize the predicted risk scores.

IV. DATA

A. Outcomes and Cohort Selection

1) *Outcomes*: The primary outcome was a composite endpoint of death, left ventricular assist device (LVAD) implantation or heart transplantation (denoted as DeLvTx). A secondary outcome of rehospitalization within 6 months of follow up was included, as rehospitalizations have been shown to be predictive of adverse outcomes [30], [31].

2) *Patient Cohorts*: This study used 5 HF cohorts, three from randomized clinical trials and two from a real-world setting of a single quaternary healthcare system. We trained the model using the ESCAPE trial [433 patients, mean age 56.1, 25.9% female], a randomized control trial studying the use of pulmonary artery catheters in severe HF patients [27].

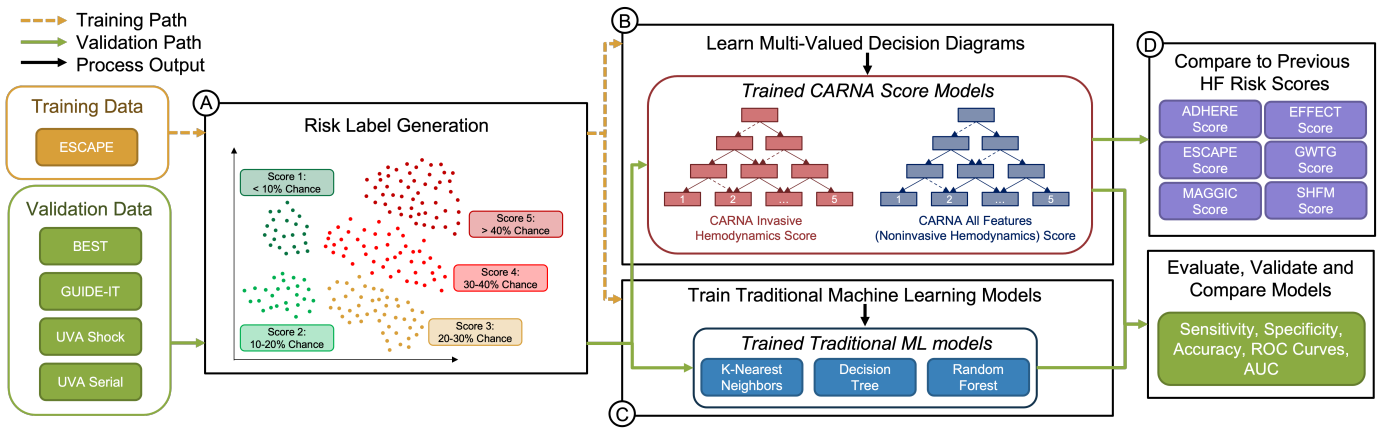


Fig. 2: Overview of CARNA Methodology. (A) The risk labels are generated using a clustering-based derivation scheme using the training and validation datasets; (B) the training data is used to train the CARNA MVDD models as well as (C) three traditional ML models for comparison. Finally, the validation data is used to evaluate the performance of the models and the resulting CARNA risk scores are compared with six previous HF risk scores (D).

The ESCAPE dataset contains a rich feature set of clinical and hemodynamic variables. Invasive hemodynamics (e.g., right atrial pressure (RAP) and pulmonary capillary wedge pressure (PCWP)) were recorded for 209 patients at baseline and prior to the removal of a heart catheter. The other 4 cohorts were used for validation: BEST [28], GUIDE-IT [29] and two real-world cohorts from University of Virginia (UVA); 1) a registry of cardiogenic shock patients, and (UVA Shock) and 2) a registry of HF patients with at least two serial right heart catheterizations for hemodynamic assessment during the same hospitalization (UVA Serial). More details are available in the cohort publications [27]–[29]. Only New York Heart Association (NYHA) functional class III-IV were included in the study to ensure comparability. Characteristics of each cohort are in Table II. Only the ESCAPE, UVA Cardiogenic Shock and UVA Serial Cardiac cohorts have invasive hemodynamics. GUIDE-IT had the highest percentage of missing data (15.07%), and ESCAPE had the highest percentage of missing hemodynamic data (12.04%).

B. Data Preprocessing

For each dataset, we first preprocessed the data, including removing outliers (necessary to reduce bias in our ML training). If the dataset had multiple temporal recordings, the values recorded at baseline and discharge were treated as two separate records. Baseline values were included (as opposed to only discharge) as they have been shown to inform a range of hemodynamic and contractile metrics and are also important in predicting outcomes as shown in previous studies, e.g., [4]. Moreover, since it was the authors’ intention to provide a single point of care risk score that could make predictions even at initial hospital admission, we included baseline measurements in the models. This also increased the total number of training/validation records, especially helpful with the small training (ESCAPE) dataset. Which cohorts had baseline and discharge data, as well as the total number of records used is reported in Table II.

Since our models support missing features, we did not impute or remove missing values from the data records. We also calculated noninvasive hemodynamics, additional metrics indicative of hemodynamic states, computed from features that were collected noninvasively. Examples include mean arterial pressure (MAP), cardiac power index (CPI), and pulse pressure (PP). These metrics were specifically selected a priori based on previous studies demonstrating incremental value in HF risk stratification [4], [32], [33]. Data was stratified into two subsets: one exploring phenotypes of invasive hemodynamics only, and the other for characterizing phenotypes between noninvasive hemodynamics and all available clinical variables including demographics, labs, and medications. Henceforth, we refer to these as the Invasive Hemodynamics and All Features feature sets, respectively.

V. METHODS

A high-level overview of the CARNA methodology is shown in Figure 2. First, the risk labels are generated (Section V-A). Agglomerative clustering is used to stratify patients in all datasets into a specified number of cluster groups and risk categories are derived for each cluster (e.g., class 1-5 ordered numerically based on actual event rates). The output of this step is a set of risk labels that indicate the probability threshold of the outcome event happening (e.g., a patient record assigned to a class of 1 indicates an outcome probability of <10% for that patient). This clustering occurred twice (once for each feature set), and the probabilities from each cluster were derived for each outcome, resulting in a total of four risk label sets. Next, using the training data (ESCAPE cohort), Multi-Valued Decision Diagrams were trained to predict the risk labels (e.g., classes 1-5, Section V-B). The trained MVDD models take in a set of features for a patient and output the predicted CARNA risk score. A total of four models were derived for each of the four risk label sets: one for each outcome (DeLVTx, Rehospitalization) and feature set (Invasive Hemodynamics, All Features) pair. Finally, the CARNA risk scores were evaluated using the four other validation cohorts

and compared with traditional ML models (Section V-C) and established HF risk scores (Section V-D) based on their predictions of the risk classes. A step-by-step walkthrough of the methodology is provided next.

A. Risk Label Generation

Each patient cohort had binary outcomes for the two endpoints (DeLvTx, rehospitalization), indicating if the outcome occurred or not. As such, there were no explicit risk thresholds for each of the patient records. Additionally, our MVDDs do not implicitly assign risk scores as a function of their learning. Since the goal of our approach was to generate a risk stratification and phenotyping score, the next step was to generate the categorical risk score values (i.e., 1–5) corresponding to real-valued outcome risks (e.g., 1 indicates a <10% risk of DeLvTx) for each record in the training and validation datasets. To this end, we reduced the dimensions of the covariates in the datasets using Principal Component Analysis (PCA) and then used a clustering approach to group patients and determine risk categorizations.

1) *PCA*: For each feature set and outcome, we performed PCA using two principal components to reduce the dimensions of the data. This was a necessary pre-step to reduce bias in the clustering, as clustering methods can be sensitive to outliers or slight changes in feature set distributions. Specifically, we use the LAPACK implementation of Singular Value Decomposition, following the PCA library available in the scikit-learn packages [34]. Since PCA cannot handle missing features, we imputed any missing values with the feature mean. We note however, that the original (non-imputed) datasets were used in the MVDD training steps later to ensure the models learned from the datasets with missing data. Importantly, the risk scores generated from this step were the labels used to train the MVDD models.

2) *Hierarchical Clustering*: Next, we clustered the patients into a specified number of groups using Agglomerative Clustering, a form of hierarchical clustering. Since the number of groups, k , is a hyperparameter, the users can select how many groups they wish to stratify the patients into. We argue this is an advantage of our approach because, based on details of the patient cohort being trained on or other user criteria (e.g., a clinician wish for only three risk groups), the number of risk groups can be adaptively selected. For our experimental purposes, we selected k as the optimal number of groups using the “Elbow” method, in which the sum of squares at each number of clusters is plotted on a graph [35]. The point on the graph where the slope changes from steep to shallow (“elbow” of the graph) indicates the optimal number of clusters to use. The clustering was performed across all datasets (including the four validation cohorts). In order to discriminate how well separated the clusters were, we computed the Hubert & Levin C Index for each feature set [36]. The C Index provides a metric to compare the dispersion of clusters compared to the overall dataset dispersion [37]. C Index should be minimized; a smaller index indicates more distinct (stable) clusters. Each cluster corresponds to one score value (e.g., five clusters for five score value assignments).

3) *Derive Outcome Probabilities*: From there, the outcome probability ranges for each score cluster were derived by computing the ground truth probability of the denoted outcome from the patients in each cluster. For example, cluster 1, corresponding to a score value of 1, had a ground truth probability of 0.041 for the DeLvTx outcome and Invasive Hemodynamics feature set; an outcome probability of <10% was derived. As a sanity check to ensure the derived score categories corresponded to the ground truth outcome probabilities across all the datasets, we reported the actual probabilities for each dataset in the Results. Finally, the score labels were assigned to each data record based on the associated cluster (e.g., a record in cluster 1 is assigned a score of 1). Using this process, we generated the risk score (labels) separately for each outcome and feature set, resulting in a total of four risk score label sets.

4) *Label Method Reasoning*: We decided to use this clustering approach because, in addition to risk stratifying patients, it uses an unsupervised method to holistically group patients, i.e., autonomously groups patients based on similar characteristics. This is highly advantageous over manually stratifying patients; manually grouping patients into risk groups is nontrivial due to large (potentially conflicting) sets of features and high variability in the presentation of patient conditions. Moreover, manual grouping is labor intensive (e.g., would require many clinician hours to characterize every patient’s risk).

B. Learning Multi-Valued Decision Diagrams

1) *Overall Training Details*: As a reminder, the MVDDs were trained on the risk score labels (i.e., classes 1–5) generated during the previous step and the risk score labels indicate probability categories of outcomes. The resulting trained models take in a set of features for a patient and output the predicted CARNA risk score. All MVDDs were learned using an independent training set (ESCAPE dataset). To maximize the training capabilities of the small dataset, we used 5-fold cross validation, in which 80% of the data in the split was used for training and the other 20% was held out for validation purposes. A total of four models were derived: one for each outcome (DeLvTx, Rehospitalization) and feature set (Invasive Hemodynamics and All Features) pair.

2) *MVDD Learning Process*: Each MVDD was learned using a training process similar to the Iterative Dichotomiser 3 (ID3) multi-class decision tree algorithm [38]. Specifically, we learn a multi-class tree using the splitting criterion of gini index or entropy. Each time we add a node to the tree, we replace the boolean edge with logical operators (“and”, “or”) and select the operator that gives the best performance (e.g., lowest gini or entropy.) The MVDDs were trained iteratively until model convergence. The implementation was developed de novo in Python3 using publicly available packages [34].

3) *Validating the MVDDs*: After model training, we independently validated the models using the four other cohorts, which had not been used in the training phase. To assess the performance of our MVDDs, five receiver operator characteristic curves (ROC) for each risk class were plotted for each model based on the ground truth risk classes in the validation datasets. If the predicted risk class matched the

Fig. 3: Example CARNA Web Portal – interface for predicting the invasive hemodynamic risk score.

ground truth risk class, this was considered a success for the ROC analysis. For example, in the case of class 1 patients, if the MVDD predicted class 1, it was considered a success, and if it predicted another class, it was considered a failure. The ROC curves were then constructed based on predictions of the risk classes, which is different from the conventional ROC method of predicting an actual event. To measure the overall model performance (e.g., as a summary metric across all risk classes), we report a single averaged area under the curve (AUC) metric, calculated by taking the weighted average of the AUCs from each risk class, weighted by the number of individuals in each class. We also calculated accuracy, sensitivity and specificity in a similar manner. We note that ROC/AUC were used over a reclassification analysis due to limitations associated with reclassification such as systematic miscalibration on validation cohorts [39].

C. Comparison to Traditional Machine Learning Models

We compared the performance of CARNA models with traditional ML models, including K-nearest neighbors (KNN), Decision Trees (DT) and Random Forests (RF). Median imputation was used for any missing values. We followed the same training procedure used for the MVDDs; each model was trained on the ESCAPE dataset using 5-fold cross validation with a 80-20% split for training/validation. Performance was computed using the same metrics on the four validation cohorts. Additionally, to assess the concordance between the predicted risk and the ground truth outcomes, calibration plots were computed, using a bin size of 10.

D. Comparison to Other Heart Failure Risk Scores

For benchmark comparison, we compared our CARNA risk score models with six other established HF risk scores: ADHERE [24], EFFECT [20], ESCAPE [23], GWTG [21], MAGGIC [22], and SHFM [7]. We limited our comparison to the models predicting risk of mortality with similar feature sets and patient cohorts. In particular, we exclude scores that use biomarkers and pathology based features (e.g., QRS measurements) since those were not available in our cohorts. Since the comparison scores cannot handle missing data, missing

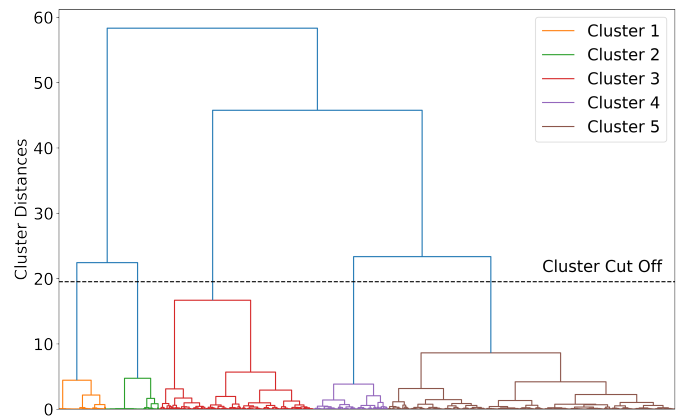


Fig. 4: Agglomerative Clustering Dendrogram for All Features feature set. Clusters are separated by horizontally dividing the top of the hierarchy based on the specified number of groups (5 in our case); this is illustrated by the horizontal dashed black line in the figures. Each leaf (end of the dendrogram) represents an individual data point.

values were imputed with the median. For each validation dataset, the predicted probability of an event was obtained from each score for each patient, and then a predicted class was assigned based on that probability. In other words, if the predicted probability of the event from the SHFM was 5% for a patient, we would say the SHFM predicted class 1, which had a probability range of 0-10% for an event. The accuracy of these other models for predicting the risk class (not the actual event) was again used for the comparison ROC analysis. To compare the AUCs between the established HF risk scores and CARNA, we performed hypothesis testing using the DeLong approach [40]. We report the scores' AUCs, the change in AUCs (CARNA AUC – other score AUC) and the p-value.

E. Open Source Tool Implementation

In order to promote open science, CARNA is an open source, extensible framework that others can easily use and build off of. Our implementation is developed in Python 3 using open source libraries. The tool package is clearly commented and includes a jupyter notebook runner file such that others can quickly and easily explore, extend, or prototype on top of the tool. In addition, our implementation includes a deployed web server which provides a live risk score prediction for ease of clinical use. An example web portal image is in Figure 3. All code is publicly available from the Github repository: <https://github.com/jozieLamp/CARNA>, and the live web server may be accessed here: <http://hemopheno.pythonanywhere.com/>.

VI. RESULTS

A. Risk Label Generation Results

From the elbow plots, 5 was chosen as the optimal number of cluster groups corresponding to 5 risk categories. An example dendrogram displaying the cluster splits for the All Features feature set is shown in Figure 4. In hierarchical

TABLE III: Risk Score Meaning and Ground Truth Risk Probabilities

DeLvTx Outcome

| Risk Score | Probability | Risk Category | Invasive Hemodynamics Cluster Means | | | | All Features Cluster Means | | | | | |
|------------|-------------|---------------------|-------------------------------------|--------|-----------|------------|----------------------------|--------|-------|----------|-----------|------------|
| | | | Overall | ESCAPE | UVA Shock | UVA Serial | Overall | ESCAPE | BEST | GUIDE-IT | UVA Shock | UVA Serial |
| 1 | <10% | Low | 0.041 | 0.081 | N/A | 0.0 | 0.043 | 0.042 | 0.0 | 0.076 | 0.048 | 0.048 |
| 2 | 10 - 20% | Low - Intermediate | 0.176 | 0.185 | N/A | 0.167 | 0.145 | 0.129 | 0.159 | 0.143 | 0.167 | 0.125 |
| 3 | 20 - 30% | Intermediate | 0.245 | 0.25 | 0.227 | 0.259 | 0.255 | 0.265 | 0.275 | 0.235 | 0.201 | 0.299 |
| 4 | 30 - 40% | Intermediate - High | 0.364 | 0.39 | 0.31 | 0.392 | 0.343 | 0.333 | 0.331 | 0.253 | 0.315 | 0.485 |
| 5 | >40% | High | 0.535 | 0.429 | 0.651 | 0.525 | 0.688 | 0.769 | 0.333 | 0.338 | 1.0 | 1.0 |

Rehospitalization Outcome

| Risk Score | Probability | Risk Category | Invasive Hemodynamics Cluster Means | | | | All Features Cluster Means | | | | | |
|------------|-------------|---------------------|-------------------------------------|--------|-----------|------------|----------------------------|--------|-------|----------|-----------|------------|
| | | | Overall | ESCAPE | UVA Shock | UVA Serial | Overall | ESCAPE | BEST | GUIDE-IT | UVA Shock | UVA Serial |
| 1 | <10% | Low | 0.025 | 0.05 | N/A | 0.0 | 0.035 | 0.077 | 0.05 | 0.017 | 0.0 | 0.031 |
| 2 | 10 - 20% | Low - Intermediate | 0.102 | 0.203 | N/A | 0.0 | 0.163 | 0.186 | 0.125 | 0.177 | 0.173 | 0.156 |
| 3 | 20 - 30% | Intermediate | 0.261 | 0.276 | 0.216 | 0.291 | 0.286 | 0.309 | 0.275 | 0.259 | 0.275 | 0.312 |
| 4 | 30 - 40% | Intermediate - High | 0.379 | 0.407 | 0.431 | 0.30 | 0.342 | 0.333 | 0.312 | 0.405 | 0.332 | 0.328 |
| 5 | >40% | High | 0.779 | 0.647 | 0.798 | 0.892 | 0.724 | 0.667 | 0.632 | 0.571 | 0.75 | 1.0 |

Tables display risk scores with corresponding outcome probability ranges and risk categories as well as cluster means, the ground truth mean outcome probability for each risk cluster in each dataset. Overall is the ground truth mean outcome probability across the entire cluster (i.e., across all datasets in the cluster). N/A = no data points assigned to that cluster; DeLvTx = composite endpoint of death, LVAD implantation or transplantation.

TABLE IV: Model Performance Summary (Validation Data)

Invasive Hemodynamic Feature Set

| Outcome | Dataset | Accuracy | Averaged AUC | Sensitivity | Specificity |
|-------------------|------------|-------------|--------------|-------------|-------------|
| DeLvTx | UVA Shock | 0.947±0.107 | 0.938±0.106 | 0.915±0.103 | 0.961±0.108 |
| | UVA Serial | 0.969±0.081 | 0.965±0.080 | 0.950±0.079 | 0.980±0.081 |
| Rehospitalization | UVA Shock | 0.907±0.102 | 0.861±0.096 | 0.791±0.086 | 0.935±0.105 |
| | UVA Serial | 0.896±0.074 | 0.896±0.074 | 0.852±0.070 | 0.940±0.078 |

All Features Feature Set

| Outcome | Dataset | Accuracy | Averaged AUC | Sensitivity | Specificity |
|-------------------|------------|-------------|--------------|-------------|-------------|
| DeLvTx | BEST | 0.997±0.037 | 0.994±0.037 | 0.990±0.037 | 0.998±0.037 |
| | GUIDE-IT | 0.997±0.070 | 0.996±0.070 | 0.995±0.069 | 0.998±0.070 |
| | UVA Shock | 0.865±0.049 | 0.871±0.050 | 0.811±0.045 | 0.931±0.054 |
| | UVA Serial | 0.858±0.067 | 0.871±0.068 | 0.815±0.063 | 0.927±0.073 |
| Rehospitalization | BEST | 0.997±0.037 | 0.994±0.037 | 0.990±0.037 | 0.998±0.037 |
| | GUIDE-IT | 0.997±0.070 | 0.996±0.070 | 0.995±0.069 | 0.998±0.070 |
| | UVA Shock | 0.694±0.036 | 0.533±0.015 | 0.250±0.041 | 0.816±0.046 |
| | UVA Serial | 0.890±0.070 | 0.798±0.061 | 0.653±0.044 | 0.942±0.075 |

Table displays value ± confidence interval. DeLvTx = composite endpoint of death, LVAD implantation or transplantation.

clustering methods, clusters are separated by horizontally dividing the top of the hierarchy based on the specified number of groups, illustrated by the horizontal dashed black line in the figures. **Our clusters are distinct with a high degree of separation, with low C Indexes of 0.063 for the Hemodynamics feature set and 0.051 for the All Features feature set.**

Table III reports the risk score meaning and corresponding real-valued average risk probabilities for each score category across all feature sets and outcomes. For example, for the Hemodynamics feature set and the DeLvTx outcome, a risk score of 3 indicates a 20–30% chance of the outcome, with a mean outcome probability of 0.245 computed from the patients in this cluster. For a sanity check, we also reported the average risk probabilities for each dataset individually. **These results**

provide evidence that the risk ranges correspond to the real observed risk in the patient cohorts.

B. Learned MVDDs

We generated a total of four MVDD models for each of the feature sets (Invasive Hemodynamics and All Features) and outcomes (DeLvTx and Rehospitalization). The Invasive Hemodynamic models use a combination of 28 features that include basic demographics, invasive and noninvasive hemodynamics; the All Features models use a combination of 66 features across demographics, labs, medications, exercise, quality metrics, other medical diagnostics and noninvasive hemodynamics. We note that these are the *maximum* number of features per model and actual prediction paths through the

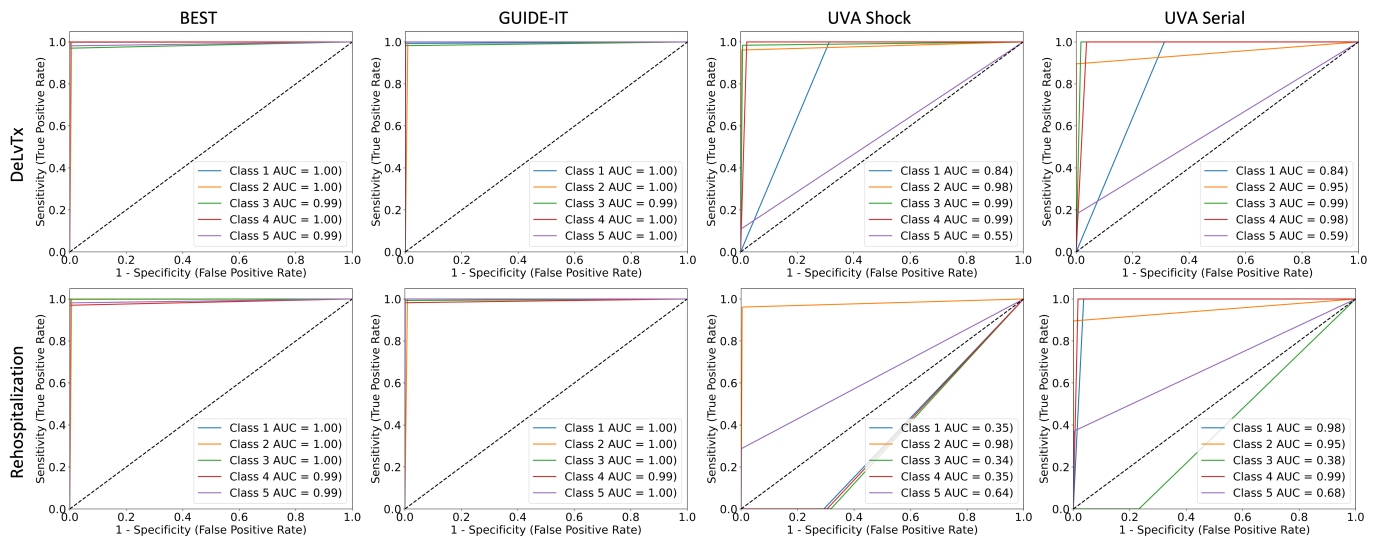


Fig. 5: ROC Curves for Validation Datasets and All Features Feature Set.

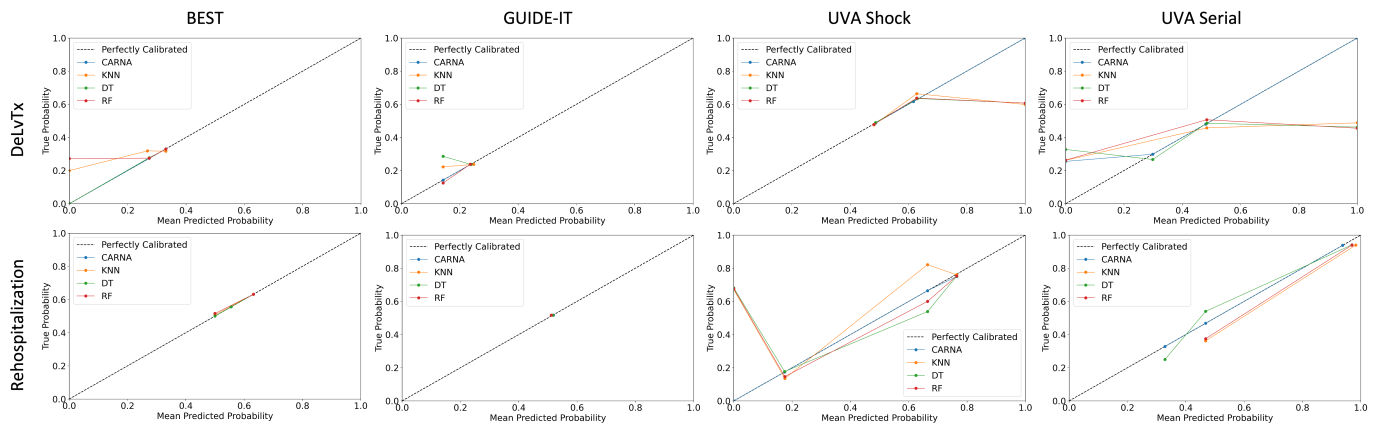


Fig. 6: Calibration Plots for All Features using a bin size of 10. True probability is the fraction of positives per bin.

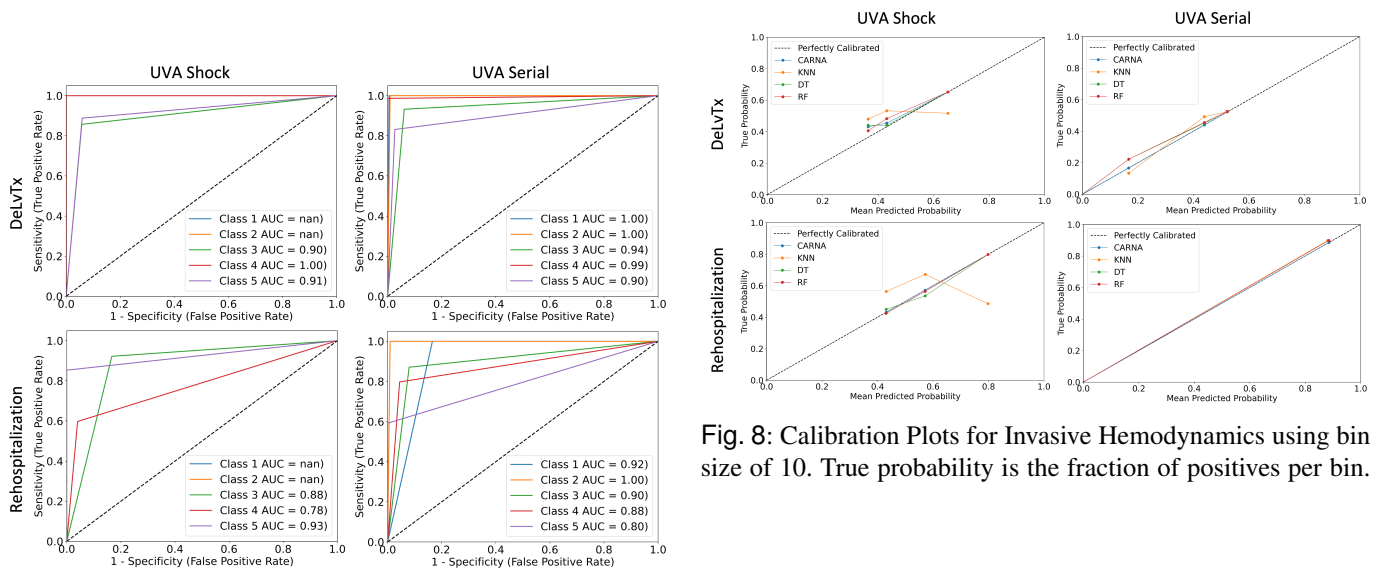


Fig. 7: ROC Curves for Validation Datasets and Invasive Hemodynamics Feature Set. nan = no data in that class.

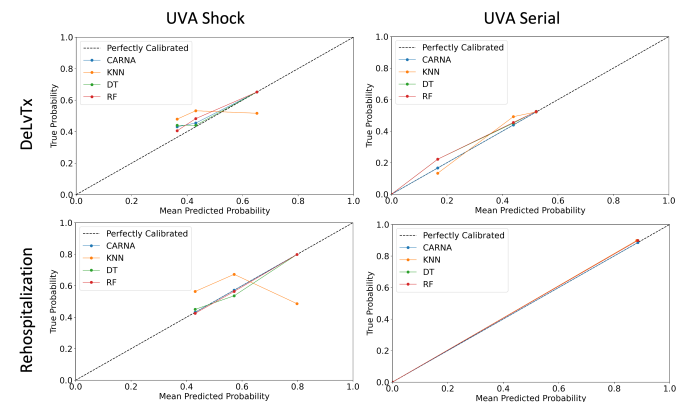


Fig. 8: Calibration Plots for Invasive Hemodynamics using bin size of 10. True probability is the fraction of positives per bin.

MVDDs use smaller subsets with interchangeable combinations of features (e.g., the features that may be “or-ed” together along a path that provide choices for which feature is used for prediction in the phenotype.)

TABLE V: CARNA Comparison to Traditional ML Models - Invasive Hemodynamics Feature Set

| DeLVTx Outcome | | | | | |
|----------------|-------|--------------------|--------------------|--------------------|--------------------|
| Dataset | Model | Accuracy | Averaged AUC | Sensitivity | Specificity |
| UVA Shock | CARNA | 0.947±0.107 | 0.938±0.106 | 0.915±0.103 | 0.961±0.108 |
| | KNN | 0.660±0.064 | 0.471±0.027 | 0.154±0.094 | 0.789±0.086 |
| | DT | 0.759±0.081 | 0.628±0.057 | 0.405±0.049 | 0.85±0.094 |
| | RF | 0.754±0.08 | 0.637±0.059 | 0.426±0.043 | 0.849±0.094 |
| UVA Serial | CARNA | 0.969±0.081 | 0.965±0.080 | 0.950±0.079 | 0.980±0.081 |
| | KNN | 0.685±0.051 | 0.5±0.001 | 0.199±0.065 | 0.801±0.065 |
| | DT | 0.776±0.062 | 0.649±0.045 | 0.438±0.029 | 0.86±0.071 |
| | RF | 0.772±0.061 | 0.628±0.042 | 0.4±0.037 | 0.855±0.07 |

| Rehospitalization Outcome | | | | | |
|---------------------------|-------|--------------------|--------------------|--------------------|--------------------|
| Data Set | Model | Accuracy | Averaged AUC | Sensitivity | Specificity |
| UVA Shock | CARNA | 0.907±0.102 | 0.861±0.096 | 0.791±0.086 | 0.935±0.105 |
| | KNN | 0.66±0.064 | 0.471±0.027 | 0.154±0.094 | 0.789±0.086 |
| | DT | 0.759±0.081 | 0.628±0.057 | 0.405±0.049 | 0.85±0.094 |
| | RF | 0.754±0.08 | 0.637±0.059 | 0.426±0.043 | 0.849±0.094 |
| UVA Serial | CARNA | 0.896±0.074 | 0.896±0.074 | 0.852±0.070 | 0.940±0.078 |
| | KNN | 0.685±0.051 | 0.5±0.001 | 0.199±0.065 | 0.801±0.065 |
| | DT | 0.776±0.062 | 0.649±0.045 | 0.438±0.029 | 0.86±0.071 |
| | RF | 0.772±0.061 | 0.628±0.042 | 0.4±0.037 | 0.855±0.07 |

Table reports value±confidence interval, bolded values indicate highest scoring item in each block. KNN = K-Nearest Neighbor; DT = Decision Tree, RF = Random Forest; DeLVTx = composite endpoint of death, LVAD implantation or transplantation.

1) *MVDD Performance*: Table IV presents the validation performance summary. The UVA Cardiogenic Shock and Serial Cardiac cohorts were used to validate the invasive hemodynamics models, since they were the only cohorts with invasive hemodynamics; all 4 validation cohorts were used to validate the All Features models. Figures 5 and 7 show the ROC curves and AUC values for each risk class for the All Features and Invasive Hemodynamics sets, respectively. For the Invasive Hemodynamics feature set across all outcomes, our validation models performed well with averaged AUCs of $0.861±0.096$ to $0.965±0.080$. For the All Features set across all datasets, our models performed well for the DeLVTx outcome with averaged AUCs of $0.871±0.068$ to $0.996±0.070$ and moderately for the rehospitalization outcome with averaged AUCs of $0.533±0.015$ to $0.996±0.070$. **These validation results provide evidence that the CARNA models yield robust risk stratification.**

C. Comparison to Traditional ML Models

For additional comparison, the performance of the CARNA models was compared with traditional ML models, including K-Nearest Neighbors (KNN), Decision Trees (DT) and Random Forests (RF), reported in Table V and VI for the Invasive Hemodynamic and All Features feature sets, respectively. Calibration plots are also shown in Figures 6 and 8. Some bins have no samples, hence why some plots do not have complete points in the line graphs. Of the traditional models, RFs followed by DTs tend to perform the best. **Across all feature sets, outcomes and datasets, the CARNA models outperform traditional ML models.**

D. Comparison to Previous HF Risk Scores

Benchmark comparison between the CARNA risk scores and 6 other previously developed HF risk scores are shown

TABLE VI: CARNA Comparison to Traditional ML Models - All Features Feature Set

| DeLVTx Outcome | | | | | |
|----------------|-------|--------------------|--------------------|--------------------|--------------------|
| Data Set | Model | Accuracy | Averaged AUC | Sensitivity | Specificity |
| BEST | CARNA | 0.997±0.037 | 0.994±0.037 | 0.990±0.037 | 0.998±0.037 |
| | KNN | 0.822±0.03 | 0.677±0.022 | 0.525±0.008 | 0.83±0.03 |
| | DT | 0.831±0.03 | 0.652±0.021 | 0.469±0.009 | 0.835±0.03 |
| | RF | 0.844±0.031 | 0.722±0.025 | 0.602±0.017 | 0.842±0.031 |
| GUIDE-IT | CARNA | 0.997±0.070 | 0.996±0.070 | 0.995±0.069 | 0.998±0.070 |
| | KNN | 0.849±0.058 | 0.575±0.027 | 0.295±0.045 | 0.854±0.059 |
| | DT | 0.852±0.058 | 0.572±0.026 | 0.277±0.047 | 0.866±0.06 |
| | RF | 0.955±0.067 | 0.719±0.046 | 0.475±0.016 | 0.964±0.067 |
| UVA Shock | CARNA | 0.865±0.049 | 0.871±0.050 | 0.811±0.045 | 0.931±0.054 |
| | KNN | 0.349±0.032 | 0.391±0.027 | 0.042±0.055 | 0.624±0.029 |
| | DT | 0.386±0.028 | 0.319±0.035 | 0.135±0.049 | 0.596±0.025 |
| | RF | 0.604±0.026 | 0.377±0.029 | 0.016±0.057 | 0.771±0.042 |
| UVA Serial | CARNA | 0.858±0.067 | 0.871±0.068 | 0.815±0.063 | 0.927±0.073 |
| | KNN | 0.346±0.044 | 0.409±0.034 | 0.022±0.077 | 0.612±0.037 |
| | DT | 0.459±0.023 | 0.383±0.038 | 0.208±0.061 | 0.596±0.035 |
| | RF | 0.339±0.045 | 0.4±0.035 | 0.009±0.079 | 0.606±0.037 |

| Rehospitalization Outcome | | | | | |
|---------------------------|-------|--------------------|--------------------|--------------------|--------------------|
| Data Set | Model | Accuracy | Averaged AUC | Sensitivity | Specificity |
| BEST | CARNA | 0.997±0.037 | 0.994±0.037 | 0.990±0.037 | 0.998±0.037 |
| | KNN | 0.822±0.03 | 0.677±0.022 | 0.525±0.008 | 0.83±0.03 |
| | DT | 0.831±0.03 | 0.652±0.021 | 0.469±0.009 | 0.835±0.03 |
| | RF | 0.844±0.031 | 0.722±0.025 | 0.602±0.017 | 0.842±0.031 |
| GUIDE-IT | CARNA | 0.997±0.070 | 0.996±0.070 | 0.995±0.069 | 0.998±0.070 |
| | KNN | 0.611±0.033 | 0.646±0.038 | 0.489±0.01 | 0.803±0.054 |
| | DT | 0.612±0.033 | 0.582±0.028 | 0.369±0.036 | 0.794±0.053 |
| | RF | 0.611±0.033 | 0.623±0.035 | 0.446±0.023 | 0.801±0.054 |
| UVA Shock | CARNA | 0.694±0.036 | 0.533±0.015 | 0.250±0.041 | 0.816±0.046 |
| | KNN | 0.349±0.032 | 0.391±0.027 | 0.042±0.055 | 0.624±0.029 |
| | DT | 0.386±0.028 | 0.319±0.035 | 0.135±0.049 | 0.596±0.025 |
| | RF | 0.604±0.026 | 0.377±0.029 | 0.016±0.057 | 0.771±0.042 |
| UVA Serial | CARNA | 0.890±0.070 | 0.798±0.061 | 0.653±0.044 | 0.942±0.075 |
| | KNN | 0.346±0.044 | 0.409±0.034 | 0.022±0.077 | 0.612±0.037 |
| | DT | 0.459±0.023 | 0.383±0.038 | 0.208±0.061 | 0.596±0.035 |
| | RF | 0.339±0.045 | 0.4±0.035 | 0.009±0.079 | 0.606±0.037 |

Table reports value±confidence interval, bolded values indicate highest scoring item in each block. KNN = K-Nearest Neighbor; DT = Decision Tree, RF = Random Forest; DeLVTx = composite endpoint of death, LVAD implantation or transplantation.

in Table VII. The table reports the AUCs for each of the HF risk scores on all datasets. Table VIII displays results of the hypothesis testing between CARNA and previous scores. The delta AUC and p-values are reported; a p-value of <0.05 indicates there is a significant difference between the two scores. **CARNA outperforms all previous HF risk scores.**

VII. DISCUSSION

In this paper, we developed an explainable ML approach using Multi-Valued Decision Diagrams to derive and validate a novel HF risk score that incorporates invasive hemodynamic and other clinical variables to stratify risk of adverse outcomes in advanced HF patients. The CARNA risk scores were highly predictive of adverse outcomes in a broad spectrum of HF patients. Accurately identifying high-risk advanced HF patients early on is fundamental for timely allocation of life-saving therapies and improvement of patient outcomes.

1) *Study Strengths*: This study has several strengths relative to previous approaches. First, our models use a richer, more diverse feature set, beyond what is used in many other clinical risk scores. Second, the use of both invasive and noninvasive hemodynamics provides incremental utility in outcome prediction, as evidenced by robust validation metrics. Third, we

TABLE VII: Comparison to Previous Scores - AUC for Outcome Mortality

| Score | Median Follow-Up | Dataset | | | | |
|-----------------|------------------|--------------------|--------------------|--------------------|--------------------|--------------------|
| | | ESCAPE | BEST | GUIDE-IT | UVA Shock | UVA Serial |
| CARNA - Hemo | 6 months | 0.952±0.091 | N/A | N/A | 0.938±0.106 | 0.965±0.080 |
| CARNA - All Fts | 6 months | 0.978±0.065 | 0.994±0.037 | 0.996±0.070 | 0.871±0.050 | 0.871±0.068 |
| ADHERE [24] | 5.85 days | 0.595±0.029 | 0.576±0.015 | 0.601±0.021 | 0.526±0.013 | 0.574±0.030 |
| EFFECT 30D [20] | 30 days | 0.550±0.021 | 0.610±0.018 | 0.635±0.024 | 0.584±0.024 | 0.610±0.037 |
| EFFECT Y1 [20] | 1 year | 0.548±0.021 | 0.638±0.020 | 0.632±0.024 | 0.612±0.027 | 0.644±0.043 |
| ESCAPE [23] | 6 months | 0.681±0.057 | 0.587±0.016 | 0.715±0.043 | 0.595±0.025 | 0.565±0.029 |
| GWTG [21] | 4 days | 0.601±0.030 | 0.538±0.010 | 0.537±0.013 | N/A | N/A |
| MAGGIC Y1 [22] | 2.5 years | 0.640±0.035 | N/A | 0.689±0.029 | 0.678±0.034 | N/A |
| MAGGIC Y3 [22] | 2.5 years | 0.640±0.035 | N/A | 0.689±0.029 | 0.678±0.034 | N/A |
| SHFM Y1 [7] | 1 year | 0.623±0.033 | 0.613±0.018 | 0.623±0.023 | 0.587±0.024 | 0.588±0.033 |
| SHFM Y3 [7] | 3 years | 0.623±0.033 | 0.616±0.018 | 0.625±0.023 | 0.588±0.024 | 0.584±0.032 |
| SHFM Y5 [7] | 5 years | 0.622±0.033 | 0.615±0.018 | 0.619±0.023 | 0.573±0.022 | 0.579±0.032 |

Table displays AUC±confidence interval; bolded values indicate highest performing score for each dataset. N/A = score could not be calculated for the dataset; Hemo = Invasive Hemodynamic; All Fts = All Features; 30D = 30-day mortality; Y1 = 1 year mortality; Y3 = 3 year mortality; Y5 = 5 year mortality.

TABLE VIII: Hypothesis Testing Between CARNA and Comparison HF Scores

| Score | Invasive Hemodynamic Feature Set | | | All Features Feature Set | | | | |
|-----------------|----------------------------------|----------------|---------------|--------------------------|----------------|----------------|----------------|---------------|
| | ESCAPE | Dataset | | ESCAPE | BEST | Dataset | | |
| | | UVA Shock | UVA Serial | | | GUIDE-IT | UVA Shock | UVA Serial |
| ADHERE [24] | -0.357, 0.262 | -0.412, <0.001 | -0.391, 0.413 | -0.383, 0.031 | -0.418, <0.001 | -0.395, 0.005 | -0.345, <0.001 | -0.297, 0.413 |
| EFFECT 30D [20] | -0.402, 0.881 | -0.354, <0.001 | -0.355, 0.315 | -0.163, 0.020 | -0.428, <0.001 | -0.384, 0.069 | -0.361, <0.001 | -0.287, 0.315 |
| EFFECT Y1 [20] | -0.404, 0.832 | -0.326, <0.001 | -0.321, 0.028 | -0.430, 0.026 | -0.356, <0.001 | -0.364, 0.096 | -0.259, <0.001 | -0.227, 0.028 |
| ESCAPE [23] | -0.271, 0.008 | -0.343, <0.001 | -0.400, 0.311 | -0.297, <0.001 | -0.407, <0.001 | -0.281, <0.001 | -0.276, <0.001 | -0.306, 0.311 |
| GWTG [21] | -0.351, 0.593 | N/A | N/A | -0.377, 0.002 | -0.456, 0.001 | -0.459, 0.001 | N/A | N/A |
| MAGGIC Y1 [22] | -0.312, 0.151 | -0.260, 0.018 | N/A | -0.338, 0.094 | N/A | -0.307, 0.048 | -0.193, 0.018 | N/A |
| MAGGIC Y3 [22] | -0.312, 0.151 | -0.260, 0.018 | N/A | -0.338, 0.094 | N/A | -0.307, 0.048 | -0.193, 0.018 | N/A |
| SHFM Y1 [7] | -0.329, 0.011 | -0.351, <0.001 | -0.377, 0.784 | -0.355, <0.001 | -0.381, <0.001 | -0.373, 0.201 | -0.284, <0.001 | -0.283, 0.784 |
| SHFM Y3 [7] | -0.329, 0.012 | -0.350, <0.001 | -0.381, 0.878 | -0.355, <0.001 | -0.378, <0.001 | -0.371, 0.173 | -0.283, <0.001 | -0.287, 0.878 |
| SHFM Y5 [7] | -0.330, 0.013 | -0.365, <0.001 | -0.386, 0.996 | -0.356, <0.001 | -0.379, <0.001 | -0.377, 0.268 | -0.298, <0.001 | -0.292, 0.996 |

Table reports Δ AUC, p-value. N/A = score could not be calculated for the dataset; 30D = 30-day mortality; Y1 = 1 year mortality; Y3 = 3 year mortality; Y5 = 5 year mortality.

can make predictive decisions using incomplete data, which is particularly advantageous in clinical scenarios with missing data. Fourth, we use multiple patient cohorts to train and validate our models, compare risk ascertainment to previous HF risk scores, and compare our models with traditional ML models, which support CARNA’s application to diverse real-world patient cohorts. Finally, our ML method is explainable and interpretable; elucidation of the phenotypes used to make risk characterizations by our models allow clinicians to better understand how and why a risk score was given. These phenotypes may identify possible HF subgroups that can be further investigated in clinical studies.

2) *CARNA Outperforms Benchmarks*: As shown in Tables IV–VIII, the CARNA risk scores highly outperform previous risk scores. The CARNA Invasive Hemodynamics score was more predictive than other scores including the ESCAPE risk score which was derived on the same cohort as our training data using linear statistical methods. The CARNA All Features score also outperformed previous risk scores, with the exception of the Rehospitalization outcome for the two UVA cohorts, which performed similar to standard risk models. Moreover, as evidenced by Tables V and VI, the CARNA models outperform traditional ML models across all datasets, feature sets and outcomes. We speculate MVDDs may outperform traditional ML models due to their ability

to handle missing data.

3) *Comment on Hemodynamics*: The CARNA Invasive Hemodynamic models do better than the CARNA All Features models, which suggests that invasive hemodynamics (along with integrated metrics) improve outcome prediction for advanced HF patients. Integrated hemodynamic indices such as Cardiac Power Index, Mean Arterial Pressure, and Pulmonary Artery Pulsatility Index were highly predictive of patient outcomes. This aligns with findings from previous studies, demonstrating the incremental utility of integrated metrics in risk assessment [4], [32], [33], [41].

4) *Model Design Choices and Limitations*: Our models use single point-of-care measurements, and do not take advantage of multiple follow-up recordings. As a result, they may lose interrelations available from multiple temporal recordings (i.e., changes between measurements). However, using single measurements in our models allows for clinician ease-of-use. Furthermore, although only the “OR” nodes in the MVDD model explicitly handle missing data, we chose to use “AND/OR” MVDDs because the “OR”-only MVDDs become very large and overfit the data. We used single MVDD models for interpretability purposes throughout the project evaluation. However, ensemble approaches (e.g., ensembles of MVDDs) have been shown to outperform single model methods [42], and this will be investigated in future. Additionally, we note

that an aspect of model interpretability may be lost due to the model predicting risk classes generated from an unsupervised clustering method as opposed to predicting the binary outcome(s) directly. Even so, we believe such a tradeoff may be acceptable due to the improved ability to risk-stratify HF patients.

Despite fewer patients and shorter follow-up time (6-months) compared to other datasets, the ESCAPE trial was selected for model training because, to the best of the authors' knowledge, it is the only cohort available with detailed invasive hemodynamics derived from a well-designed randomized HF clinical trial. There is potential for selection bias by choosing trial data and higher-risk patients in the two UVA cohorts. In addition, many of our validation datasets did not have invasive hemodynamics so we were unable to validate the invasive hemodynamic models on all four of the patient cohorts. Further, there were heterogeneities in HF acuity status in the datasets used. Even so, validation of the CARNA models yielded robust risk stratification compared to other conventional HF risk score and ML models.

VIII. CONCLUSION

This study developed a novel advanced HF risk stratification using an explainable ML methodology. The CARNA risk scores are more predictive of patient outcomes than previous approaches and provide detailed characterizations of clinical phenotypes. CARNA may facilitate clinical decision making and provide robust risk stratification.

REFERENCES

- [1] S. M. Dunlay, V. L. Roger, J. M. Killian, *et al.*, "Advanced heart failure epidemiology and outcomes: A population-based study," *Heart Failure*, vol. 9, no. 10, pp. 722–732, 2021.
- [2] F. H. Verbrugge, M. Guazzi, J. M. Testani, and B. A. Borlaug, "Altered hemodynamics and end-organ damage in heart failure: Impact on the lung and kidney," *Circulation*, vol. 142, no. 10, pp. 998–1012, 2020.
- [3] L. A. Allen, L. W. Stevenson, K. L. Grady, *et al.*, "Decision making in advanced heart failure: A scientific statement from the american heart association," *Circulation*, vol. 125, no. 15, pp. 1928–1952, 2012.
- [4] K. C. Bilchick, E. Mejia-Lopez, P. McCullough, *et al.*, "Clinical impact of changes in hemodynamic indices of contractile function during treatment of acute decompensated heart failure," *Journal of cardiac failure*, vol. 24, no. 1, pp. 43–50, 2018.
- [5] S. Hsu, J. C. Fang, and B. A. Borlaug, "Hemodynamics for the heart failure clinician: A state-of-the-art review," *Journal of cardiac failure*, vol. 28, no. 1, pp. 133–148, 2022.
- [6] B. A. Borlaug and D. A. Kass, "Invasive hemodynamic assessment in heart failure," *Cardiology clinics*, vol. 29, no. 2, pp. 269–280, 2011.
- [7] W. C. Levy, D. Mozaffarian, D. T. Linker, *et al.*, "The seattle heart failure model: Prediction of survival in heart failure," *Circulation*, vol. 113, no. 11, pp. 1424–1433, 2006.
- [8] G. L. Di Tanna, H. Wirtz, K. L. Burrows, and G. Globe, "Evaluating risk prediction models for adults with heart failure: A systematic literature review," *PLoS One*, vol. 15, no. 1, e0224135, 2020.
- [9] M. Canepa, C. Fonseca, O. Chioncel, *et al.*, "Performance of prognostic risk scores in chronic heart failure patients enrolled in the european society of cardiology heart failure long-term registry," *JACC: Heart Failure*, vol. 6, no. 6, pp. 452–462, 2018.
- [10] P. Codina, J. Lupón, A. Borrellas, *et al.*, "Head-to-head comparison of contemporary heart failure risk scores," *European Journal of Heart Failure*, vol. 23, no. 12, pp. 2035–2044, 2021.
- [11] B. Greenberg, A. Brann, C. Campagnari, E. Adler, and A. Yagil, "Machine learning applications in heart failure disease management: Hype or hope?" *Current Treatment Options in Cardiovascular Medicine*, vol. 23, no. 6, p. 35, 2021.
- [12] D. Mpanya, T. Celik, E. Klug, and H. Ntsinjana, "Predicting mortality and hospitalization in heart failure using machine learning: A systematic literature review," *IJC Heart & Vasculature*, vol. 34, p. 100773, 2021.
- [13] A. Srinivasan, T. Ham, S. Malik, and R. K. Brayton, "Algorithms for discrete function manipulation," in *1990 IEEE international conference on computer-aided design*, IEEE Computer Society, 1990, pp. 92–93.
- [14] D. Bergman, A. A. Cire, W.-J. Van Hove, and J. Hooker, *Decision diagrams for optimization*. Springer, 2016, vol. 1.
- [15] A. B. Arrieta, N. Díaz-Rodríguez, J. Del Ser, *et al.*, "Explainable artificial intelligence (xai): Concepts, taxonomies, opportunities and challenges toward responsible ai," *Information fusion*, vol. 58, pp. 82–115, 2020.
- [16] S. Bharati, M. R. H. Mondal, and P. Podder, "A review on explainable artificial intelligence for healthcare: Why, how, and when?" *IEEE Transactions on Artificial Intelligence*, 2023.
- [17] S. Rao, Y. Li, R. Ramakrishnan, *et al.*, "An explainable transformer-based deep learning model for the prediction of incident heart failure," *IEEE Journal of Biomedical and Health Informatics*, vol. 26, no. 7, pp. 3362–3372, 2022.
- [18] A. Chaddad, J. Peng, J. Xu, and A. Bouridane, "Survey of explainable ai techniques in healthcare," *Sensors*, vol. 23, no. 2, p. 634, 2023.
- [19] A. M. Florio, P. Martins, M. Schiffer, T. Serra, and T. Vidal, "Optimal decision diagrams for classification," *arXiv preprint arXiv:2205.14500*, 2022.
- [20] D. S. Lee, P. C. Austin, J. L. Rouleau, P. P. Liu, D. Naimark, and J. V. Tu, "Predicting mortality among patients hospitalized for heart failure: Derivation and validation of a clinical model," *Jama*, vol. 290, no. 19, pp. 2581–2587, 2003.
- [21] P. N. Peterson, J. S. Rumsfeld, L. Liang, *et al.*, "A validated risk score for in-hospital mortality in patients with heart failure from the american heart association get with the guidelines program," *Circulation: Cardio-*

- vascular Quality and Outcomes*, vol. 3, no. 1, pp. 25–32, 2010.
- [22] S. J. Pocock, C. A. Ariti, J. J. McMurray, *et al.*, “Predicting survival in heart failure: A risk score based on 39 372 patients from 30 studies,” *European heart journal*, vol. 34, no. 19, pp. 1404–1413, 2013.
- [23] C. M. O’Connor, V. Hasselblad, R. H. Mehta, *et al.*, “Triage after hospitalization with advanced heart failure: The escape (evaluation study of congestive heart failure and pulmonary artery catheterization effectiveness) risk model and discharge score,” *Journal of the American College of Cardiology*, vol. 55, no. 9, pp. 872–878, 2010.
- [24] G. C. Fonarow, K. F. Adams, W. T. Abraham, C. W. Yancy, W. J. Boscardin, A. S. A. Committee, *et al.*, “Risk stratification for in-hospital mortality in acutely decompensated heart failure: Classification and regression tree analysis,” *Jama*, vol. 293, no. 5, pp. 572–580, 2005.
- [25] E. D. Adler, A. A. Voors, L. Klein, *et al.*, “Improving risk prediction in heart failure using machine learning,” *European journal of heart failure*, vol. 22, no. 1, pp. 139–147, 2020.
- [26] S. Angraal, B. J. Mortazavi, A. Gupta, *et al.*, “Machine learning prediction of mortality and hospitalization in heart failure with preserved ejection fraction,” *JACC: Heart Failure*, vol. 8, no. 1, pp. 12–21, 2020.
- [27] C. Binanay, R. M. Califf, V. Hasselblad, *et al.*, “Evaluation study of congestive heart failure and pulmonary artery catheterization effectiveness: The escape trial,” *Jama*, vol. 294, no. 13, pp. 1625–1633, 2005.
- [28] B.-B. E. of Survival Trial Investigators, “A trial of the beta-blocker bucindolol in patients with advanced chronic heart failure,” *New England Journal of Medicine*, vol. 344, no. 22, pp. 1659–1667, 2001.
- [29] G. M. Felker, T. Ahmad, K. J. Anstrom, *et al.*, “Rationale and design of the guide-it study: Guiding evidence based therapy using biomarker intensified treatment in heart failure,” *JACC: Heart Failure*, vol. 2, no. 5, pp. 457–465, 2014.
- [30] A. Ahmed, W. S. Aronow, and J. L. Fleg, “Higher new york heart association classes and increased mortality and hospitalization in patients with heart failure and preserved left ventricular function,” *American heart journal*, vol. 151, no. 2, pp. 444–450, 2006.
- [31] A. S. Desai and L. W. Stevenson, “Rehospitalization for heart failure: Predict or prevent?” *Circulation*, vol. 126, no. 4, pp. 501–506, 2012.
- [32] K. C. Bilchick, N. Chishinga, A. M. Parker, *et al.*, “Plasma volume and renal function predict six-month survival after hospitalization for acute decompensated heart failure,” *Cardiorenal medicine*, vol. 8, no. 1, pp. 61–70, 2018.
- [33] S. Mazimba, J. L. Kennedy, D. Zhuo, *et al.*, “Decreased pulmonary arterial proportional pulse pressure after pulmonary artery catheter optimization for advanced heart failure is associated with adverse clinical outcomes,” *Journal of cardiac failure*, vol. 22, no. 12, pp. 954–961, 2016.
- [34] F. Pedregosa, G. Varoquaux, A. Gramfort, *et al.*, “Scikit-learn: Machine learning in python, journal of machine learning research,” 2011.
- [35] R. Tibshirani, G. Walther, and T. Hastie, “Estimating the number of clusters in a data set via the gap statistic,” *Journal of the Royal Statistical Society: Series B (Statistical Methodology)*, vol. 63, no. 2, pp. 411–423, 2001.
- [36] L. J. Hubert and J. R. Levin, “A general statistical framework for assessing categorical clustering in free recall,” *Psychological bulletin*, vol. 83, no. 6, p. 1072, 1976.
- [37] Pypi. “C-index.” (), [Online]. Available: <https://pypi.org/project/c-index/#description> (visited on 2022).
- [38] J. R. Quinlan, “Induction of decision trees,” *Machine learning*, vol. 1, pp. 81–106, 1986.
- [39] M. J. Leening, M. M. Vedder, J. C. Witteman, M. J. Pencina, and E. W. Steyerberg, “Net reclassification improvement: Computation, interpretation, and controversies: A literature review and clinician’s guide,” *Annals of internal medicine*, vol. 160, no. 2, pp. 122–131, 2014.
- [40] E. R. DeLong, D. M. DeLong, and D. L. Clarke-Pearson, “Comparing the areas under two or more correlated receiver operating characteristic curves: A non-parametric approach,” *Biometrics*, pp. 837–845, 1988.
- [41] S. Mazimba, H. Mwansa, K. Breathett, *et al.*, “Systemic arterial pulsatility index (sapi) predicts adverse outcomes in advanced heart failure patients,” *Heart and Vessels*, vol. 37, no. 10, pp. 1719–1727, 2022.
- [42] M. Hosni, J. M. Carrillo de Gea, A. Idri, *et al.*, “A systematic mapping study for ensemble classification methods in cardiovascular disease,” *Artificial Intelligence Review*, vol. 54, pp. 2827–2861, 2021.